Editors' Suggestion | Featured in Physics

# Boundaries Control Collective Dynamics of Inertial Self-Propelled Robots

A. Deblais,[1] T. Barois,[1] T. Guerin,[1] P. H. Delville,[1] R. Vaudaine,[1]
J. S. Lintuvuori,[1] J. F. Boudet,[1] J. C. Baret,[2] and H. Kellay[1]
[1]*Univ. Bordeaux, CNRS, LOMA, UMR 5798, F-33405 Talence, France*
[2]*CNRS, Univ. Bordeaux, CRPP, UPR 8641, 115 Avenue Schweitzer, 33600 Pessac, France*

(Received 27 October 2017; revised manuscript received 13 February 2018; published 4 May 2018)

Simple ingredients, such as well-defined interactions and couplings for the velocity and orientation of self-propelled objects, are sufficient to produce complex collective behavior in assemblies of such entities. Here, we use assemblies of rodlike robots made motile through self-vibration. When confined in circular arenas, dilute assemblies of these rods act as a gas. Increasing the surface fraction leads to a collective behavior near the boundaries: polar clusters emerge while, in the bulk, gaslike behavior is retained. The coexistence between a gas and surface clusters is a direct consequence of inertial effects as shown by our simulations. A theoretical model, based on surface mediated transport accounts for this coexistence and illustrates the exact role of the boundaries. Our study paves the way towards the control of collective behavior: By using deformable but free to move arenas, we demonstrate that the surface induced clusters can lead to directed motion, while the topology of the surface states can be controlled by biasing the motility of the particles.

DOI: 10.1103/PhysRevLett.120.188002

A large collection of motile objects, be they natural or artificial, may show a host of complex behavior and collective dynamics [1–9]. Pioneering work on granular materials (disks or rods) rendered motile through a global vibration of the container [4,10–12] or through self-induced motility [13] showed the emergence of large number fluctuations and global properties for sufficiently large densities. Self-propelled rods in a liquid environment display global effects with direct applications to bacterial colonies or microtubules [14–17]. Small micrometer-sized motile colloidal particles or droplets illustrate the role of motility on the global behavior of particle assemblies in both experiments and theoretical modeling [18–22].

In these systems the dynamics is dominated by dissipation and inertial effects are neglected. Inertia may hinder local alignment, a key ingredient in producing collective dynamics. The role of inertia and of the absence of local alignment for collective behavior need to be examined in detail [2]. In addition, in overdamped systems, boundaries have a drastic effect on the clustering of the motile entities, as observed in both numerics and experiments [14,15,23–26], but the role of boundaries on inertial particles remains elusive.

In this Letter we focus on both of these issues. We show that boundaries favor the presence of large polar clusters while inertia and low damping favor a gas phase in the central region by limiting the accumulation of particles at the walls. This coexistence is recovered in numerical simulations and explained using a minimal model. A rich phenomenology then emerges by introducing chirality in the particle motion leading to segregation of the chiral particles in the cluster or by using free to move flexible boundaries for which the clustering couples to a global displacement of the arena confining the particles.

We use small plastic rodlike robots. Their motility is induced by the vibration of the robot itself with an embedded battery operating a vibration module working at frequencies $f$ between 150 and 60 Hz. These robots have asymmetric soft legs, which after a few vibration cycles give rise to a directed movement with velocities that depend on the frequency of vibration and can be varied from roughly $V = 20$ to 40 cm/s. The mechanism of propulsion has been described in Ref. [13]. We confine a varying number $N$ of active rods, of projected area $A$ and mean velocity $V$, in a fixed circular arena of radius $R = 30$ cm. Similarly to the experiments, numerical simulations using Langevin dynamics of self-propelled rods in the presence of low damping, inertial terms, and noise in the dynamics are performed. Comparisons between experiments and simulations are carried out for similar surface fractions $\phi$ and Péclet numbers Pe, the ratio of advection to diffusion [27]. More details on the properties of the robots and the numerics are given in Ref. [27].

At low surface fractions $\phi = (NA/\pi R^2)$, the assembly forms a disordered state, Fig. 1 (Movie 1 of Supplemental Material [27]). At higher $\phi$, large polar surface clusters, with a well-defined "hedgehog" shape [13,23,27], form and coexist with a disordered gas phase in the central area (Fig. 1 and Movie 2 of Ref. [27]). To quantify this behavior, we measure the probability distributions $P(n)$ for a randomly selected rod to be in an aggregate of size $n$ [7,27]. At low $\phi$, this probability is a monotonic and

 

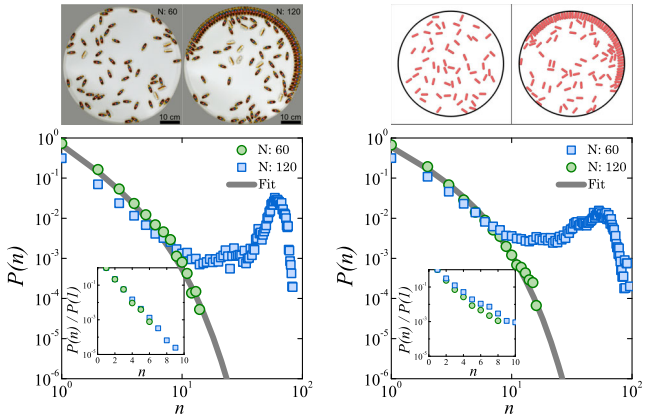


FIG. 1. Clustering transition. Left-hand panel: Experiments. Photographs of the arena ($R = 30$ cm with 1 mm thick walls) with different numbers $N$ of robots. Note the gas phase for $N = 60$, $\phi = 0.136$, and the presence of a large surface cluster for $N = 120$, $\phi = 0.273$. $P(n)$ for the gas phase for which the PDF is monotonic and the denser phase with large clusters for which the PDF is bimodal. The solid line is a fit to the functional form given in the text for the gas phase. Right-hand panel: Simulations. Photographs of the arena. Along with a plot of $P(n)$ for surface fractions $\phi$ of 0.11 and 0.22. The insets show $P(n)$ calculated for the central region only where it is monotonic and exponential. The Péclet number Pe = 31 for the experiments and Pe = 37 for the simulations. (The rendering of the images from the simulations is carried out using OVITO [33]).

decreasing function of $n$, Fig. 1, approximated as $P(n) \sim n^{-\gamma} \exp(-n/N_c)$. $N_c$, a characteristic cluster size, increases with $\phi$ and the exponent $\gamma$ is roughly 1.7 [27]. While this functional form is similar to previously measured probability distribution functions (PDFs) of clustering in other experiments and simulations, it is difficult to compare our findings to these results as the effects of boundaries are dominant in our case [16,30–32]. Further increase in $\phi$ results in a transition to polar cluster formation and a drastic change of $P(n)$, which becomes nonmonotonic with a smooth decrease for small $n$ along with a marked peak for large clusters, Fig. 1. This phenomenology is reproduced in detail by our numerical simulations, as can be seen by comparing left-hand and right-hand panels of Fig. 1 (see also Movies 3 and 4 in Supplemental Material [27]).

By examining the spatial distribution of clusters in the arena, large clusters seem to assemble near the boundaries only [27]. Removing the effect of the boundary by limiting the analysis to the central region only, the PDFs become monotonic and their functional shape changes to a simple exponential (insets of Fig. 1 and Ref. [27]). That inertial effects are important comes from simulations in the overdamped case for similar conditions as Fig. 1 (noise amplitude and surface fraction). Here no significant gas-cluster coexistence is observed [27], as the boundaries favor strong clustering at the walls in the presence of strong damping [13,23,24,26].

The observed coexistence is a direct consequence of the interplay between inertia and boundary effects. The boundaries favor the presence of clusters but inertia limits this effect. The collisions between the rods, due to the presence of inertia, do not induce local alignment in the central region, neither in experiments nor in simulations [27]. As such, the central region remains disordered while polar clusters are confined to the walls.

A simple model based on surface mediated transport [34–37] helps to rationalize these experimental results [27]. The rods are assumed to obey a diffusion equation in the gas phase in the central region. To account for boundary effects, we introduce an additional population of rods that move ballistically along the surface. The residence time of these particles at the surface is taken to be $\tau_s$. This population, which comes from the bulk with a certain attachment probability at the boundary, is assumed to be at the core of cluster formation. Once in a cluster, a particle can detach only at the cluster ends after a time $\tau_c$. Once they detach from the cluster, the particles return into the gas phase. It is interesting to note here that this model has similarities with one-dimensional models of self-propelled rods since only the particles at the boundary are considered for the clustering, with a major difference, as a bulk reservoir is present in our case [38–40].

The main result of our model is that clustering can occur only if the number of rods exceeds a threshold $N^*$. If $N > N^*$, the rods residing at the boundary reach the cluster fast enough to make it grow, whereas a small cluster will disappear when $N < N^*$. An explicit formula for $N^*$ as a function of the model parameters is given in Ref. [27], but scalings for $N^*$ can be identified. Two limiting cases arise. If $\tau_s \gg R/V$, a particle almost never detaches from the boundary before reaching the cluster leading to $N^* \sim (R/\tau_c V)$. In the opposite case $\tau_s \ll R/V$, a particle attaching to the boundary at a random position explores only a small length $\tau_s V$ before detaching, leading to $N^* \sim (R^2/\tau_c \tau_s V^2)$. In both limiting cases, the time constant $\tau_c$ plays an important role while $\tau_s$ plays a role only when it is small compared to $R/V$.

In our experiments, both $\tau_c$ and $\tau_s$ can be varied allowing us to test the model explicitly. The rods have an inherent vibration, at the frequency of vibration $f$, in the transverse direction to their directed motion [27]. This vibration has a direct effect on the collisions between rods and with the boundary. While $\tau_s$ increases slowly, $\tau_c$ increases significantly as $f$ decreases since the rod collides with less intensity with the wall and with the other rods. A similar effect is found in the simulations where the intensity of the noise controls the efficiency of clustering. In order to rationalize this effect and compare experiments, simulations, and theory, a phase diagram showing $\phi = (N^* A/\pi R^2)$ versus Pe is presented in Fig. 2. Polar clustering becomes more efficient; i.e., $\phi = (N^* A/\pi R^2)$

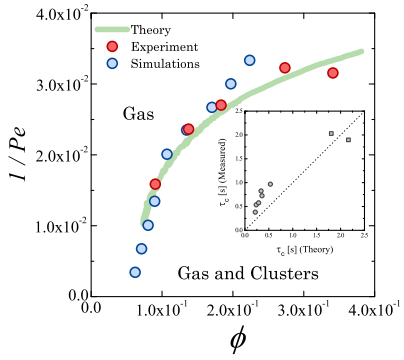


FIG. 2. Phase diagram in $\phi - \mathrm{Pe}$ representation for the experiments and the simulations. For each Pe value, the surface fraction for which a transition from gas to coexistence of gas and clusters is found. The model is given as a continuous line whereby for each Pe the value of $\phi$ for which a cluster is stable (i.e., $\phi = (N^* A/\pi R^2)$) is found. Inset: The residence time in the cluster needed to fit the phase diagram using the model compared to estimates of this timescale from experiments. Additional points from the simulations are also shown.

decreases, as Pe increases. The theoretical fit was carried out by first fitting $\tau_s$ and $\tau_c$ versus $f$. This allowed us to have a smooth functional form for these two parameters based on the experimental data in Ref. [27]. The parameters of this fit for $\tau_c$ were then left free to fit the phase diagram. We compare the values of $\tau_c$ from theory to experiment (for which several independent measurements of $\tau_c$ versus $f$ and $\phi$ were obtained) in the inset. Along with the experimental points, we have added two additional points from the numerical simulations. The agreement between the model, the experiments, and the simulations is very good, as seen in Fig. 2.

Besides the phase diagram, other avenues are explored. The robots can be modified to obtain trajectories with different chiralities [27]. Our modified rods have curved trajectories and are unlike other bots that have an inherent rotation around their main axis [41,42]. Figure 3 shows that chirality can inhibit clustering and polar ordering near the walls in our numerical simulations, where for a small additional torque which induces circular trajectories (50% of the rods rotate counterclockwise while the other 50% rotate clockwise), a higher proportion of rods ends up in the gas phase. Rods with circular trajectories have a tendency to travel shorter distances and thus have a smaller probability to reach the boundaries. Chirality clearly inhibits cluster formation and decreases both $\tau_s$ and $\tau_c$ as the rods move out of clusters and out of the boundary through rotation. In addition to damping effects, rotation is another means of changing the interplay between boundary clusters and the disordered state. On the other hand, once the cluster becomes stable (for larger $\phi$, softer walls, or smaller frequencies), the cluster seems to be made up of two distinct regions with opposite chiralities (Fig. 3 and Supplemental Material Movie 5 [27]). This chirality sorting is related to the simple effect whereby a rod, moving along the boundary in, say, the clockwise direction, with a circular trajectory in the counterclockwise direction, will remain at the boundary for longer times and has thus a higher probability of reaching the cluster on only one end [27].

Since the clustering observed depends strongly on $\tau_s$ and $\tau_c$, a change of the boundary properties, which may increase or decrease these timescales, gives the possibility of controlling collective behavior. The interaction of these rods with the boundary can be tuned through the flexibility of the walls. This increases both timescales and favors clustering even for low $\phi$, opening the possibility of generating global movement and large deformability by using a handful of active entities. The effects of flexible walls have recently attracted attention for pressure measurements of active systems as well as for shaping filaments [43,44].

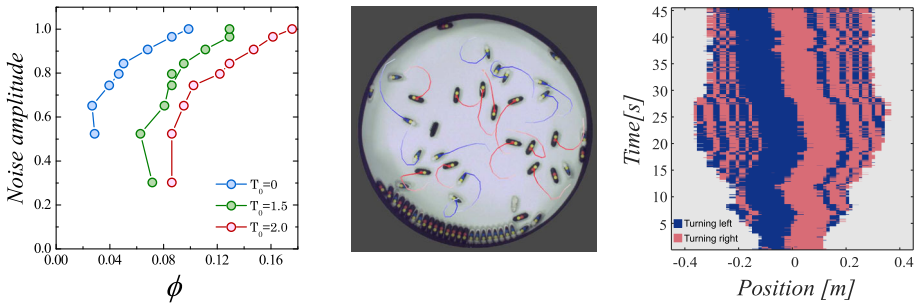


FIG. 3. Chirality effects: Left: Phase diagram from simulations summarizing the effects of an additional torque $T_0$, giving rise to circular trajectories, on the surface fraction for the transition to surface cluster formation. For these simulations, the value of the friction coefficient is 6. Middle: Photograph of an assembly of left and right turning rods. Left turning rods are marked with blue dots while right turning rods are marked with red dots. The trajectories of the rods are displayed with the direction of movement indicated by increasing color intensity. The cluster at the bottom of the image is segregated by chirality. Right: Spatiotemporal evolution from experiments where left and right turning robots segregate within the cluster as it grows in size.

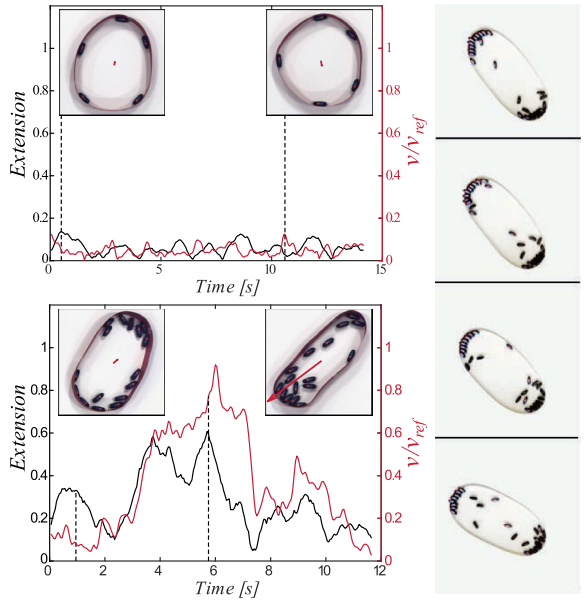


FIG. 4. Deformation of the arena and onset of locomotion of the whole cell. The deformation is small and the locomotion is limited for small $N$. For a higher $N$, the deformation is large and the mobility of the arena is strong with velocities near those of the rods. The deformation is measured as $2(a-b)/p$, where $a$ is the long axis, $b$ the small axis, and $p$ the perimeter of the arena. The velocity of the center of mass of the arena is normalized by the mean velocity of the individual rods. The correlation between deformation and locomotion is near 0.72 for the higher $N$. The arena is made of 0.1 mm thick paper with $R = 10.5$ cm. The photographs to the right illustrate that large deformations are not strictly correlated to locomotion as the presence of two clusters on each end balance the arena in a static position.

When the container walls are flexible and free to move, the presence of the polar clusters gives rise to large deformations and translational motion of the arena, Fig. 4. Here, the arena, $R = 10.5$ cm, is made of 0.1 mm paper and is left free to move as opposed to the arena used above, which is rigid (1 mm thickness) and fixed to the table. Different surface fractions are used to examine how and when the mobility of the container and corresponding change of shape set in. In Fig. 4, we plot the measured mean velocity of the arena for two different surface fractions. For small surface fractions, the arena has no directed motion and its shape remains roughly circular. The rods are confined parallel to the surface and may reside there for long times. For larger $\phi$, the arena becomes elongated and moves at persistent speed, comparable to the speed of individual rods. This symmetry breaking transition and the associated mobility is a novel effect and calls for additional work. For even higher $\phi$, not one but two different clusters may be present. In this case, the deformation can reach large values when the two clusters point in opposite directions, Fig. 4. This configuration moves if the two clusters are not symmetric and remains static otherwise. Even though the mobility of the arena and its deformation may be correlated, this correlation is dependent on the configuration of the clusters present. Note that the presence of the cluster is also accompanied by a large curvature of the arena. The interplay between curvature and clustering has been examined theoretically for overdamped rods [45]. Further, our own theoretical framework can be modified, through a dependence of the two timescales on the flexibility of the boundaries, to model such peculiar effects.

The link between flexibility and mobility can be used to implement self-adaptive containers capable of going around obstacles and corners or entering small spaces as seen in Fig. 5 (Supplemental Material Movies 6A and 6B [27]). Here, we use a longer perimeter for the flexible arena which has a radius of 21 cm. In Fig. 5, the formation of the aggregate makes the arena mobile which, after a certain time, encounters an aperture. As it moves along one of the obstacles forming the aperture, it reaches the outlet and manages to deform considerably and go through in a matter of roughly 10 s. In Fig. 5, the same arena encounters a circular obstacle. This encounter leads to a large deformation of the boundary, which ends up surrounding the obstacle and rotating around it by adapting its shape.

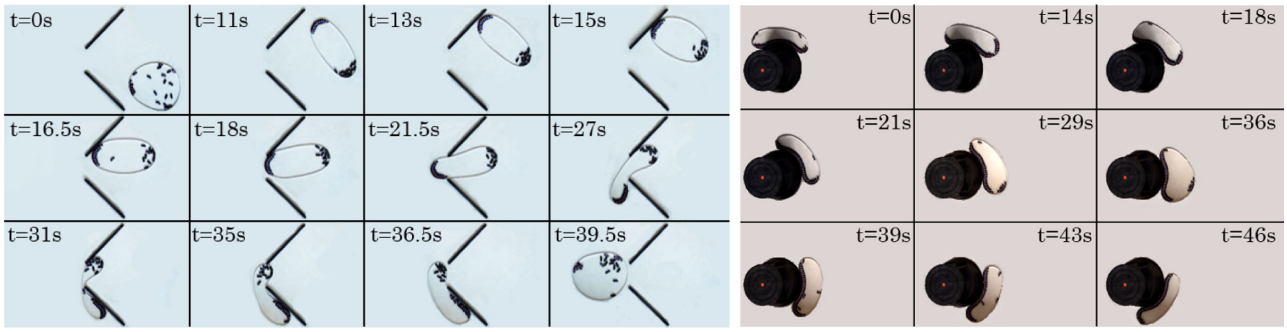


FIG. 5. Collective motion. For a flexible arena made of a boundary with 0.1 mm thick steel walls with $R = 21$ cm, the rods reside longer at the surface and form a cluster relatively quickly, deform the arena, and set it in motion to go through an aperture (left series) or go around an obstacle (right series). For each case, a time series is shown.

This Letter presents a new system where the interplay between the dynamics of the individual rods and the boundaries gives rise to cluster formation, collective behavior, and a host of interesting dynamics. Understanding and controlling this dynamics is crucial in designing systems, with tunable properties, consisting of a multitude of small motile entities or robots. The simplicity of the system allows us to introduce nontrivial effects such as curved trajectories leading to chirality sorting through confinement. The flexibility of the arena is shown to produce large deformations resembling biological entities allowing the assembly to go through apertures and around corners. These results pave the way to applications for the design of new soft robots with improved or programmable motility.

H. K. thanks the Institut Universitaire de France for partial support.

[1] G. Popkin, Nature (London) **529**, 16 (2016).
[2] C. Bechinger, R. Di Leonardo, H. Lwen, C. Reichhardt, G. Volpe, and G. Volpe, Rev. Mod. Phys. **88**, 045006 (2016).
[3] T. Vicsek and A. Zafeiris, Phys. Rep. **517**, 71 (2012).
[4] V. Narayan, S. Ramaswamy, and N. Menon, Science **317**, 105 (2007).
[5] D. Saintillan and M. J. Shelley, *Complex Fluids in Biological Systems* (Springer, New York, 2015), pp. 319–355.
[6] Y. Sumino, K. H. Nagai, Y. Shitaka, D. Tanaka, K. Yoshikawa, H. Chaté, K. Oiwa, and Y. Sumino, Nature (London) **483**, 448 (2012).
[7] F. Peruani, Eur. Phys. J. Spec. Top. **225**, 2301 (2016).
[8] M. E. Cates and J. Tailleur, Annu. Rev. Condens. Matter Phys. **6**, 219 (2015).
[9] A. P. Solon, Y. Fily, A. Baskaran, M. E. Cates, Y. Kafri, M. Kardar, and J. Tailleur, Nat. Phys. **11**, 673 (2015).
[10] N. Kumar, H. Soni, S. Ramaswamy, and A. K. Sood, Nat. Commun. **5**, 4688 (2014).
[11] J. Deseigne, O. Dauchot, and H. Chaté, Phys. Rev. Lett. **105**, 098001 (2010).
[12] A. Kudrolli, G. Lumay, D. Volfson, and L. S. Tsimring, Phys. Rev. Lett. **100**, 058001 (2008).
[13] L. Giomi, N. Hawley-Weld, and L. Mahadevan, Proc. R. Soc. A **469**, 20120637 (2013).
[14] H. Wioland, F. G. Woodhouse, J. Dunkel, J. O. Kessler, and R. E. Goldstein, Phys. Rev. Lett. **110**, 268102 (2013).
[15] E. Lushi, H. Wioland, and R. Goldstein, Proc. Natl. Acad. Sci. U.S.A. **111**, 9733 (2014).
[16] F. Peruani, J. Starruss, V. Jakovljevic, L. Sogaard-Andersen, A. Deutsch, and M. Bar, Phys. Rev. Lett. **108**, 098102 (2012).
[17] T. Sanchez, D. T. N. Chen, S. J. DeCamp, M. Heymann, and Z. Dogic, Nature (London) **491**, 431 (2012).
[18] A. Bricard, J.-B. Caussin, N. Desreumaux, O. Dauchot, and D. Bartolo, Nature (London) **503**, 95 (2013).
[19] A. Bricard, J.-B. Caussin, D. Das, C. Savoie, V. Chikkadi, K. Shitara, O. Chepizhko, F. Peruani, D. Saintillan, and D. Bartolo, Nat. Commun. **6**, 7470 (2015).
[20] C. Lozano, B. Hagen, H. Löwen, and C. Bechinger, Nat. Commun. **7**, 12828 (2016).
[21] I. Theurkauff, C. Cottin-Bizonne, J. Palacci, C. Ybert, and L. Bocquet, Phys. Rev. Lett. **108**, 268303 (2012).
[22] F. Ginot, I. Theurkauff, D. Levis, C. Ybert, L. Bocquet, L. Berthier, and C. Cottin-Bizonne, Phys. Rev. X **5**, 011004 (2015).
[23] H. H. Wensink and H. Löwen, Phys. Rev. E **78**, 031409 (2008).
[24] A. Kaiser, H. H. Wensink, and H. Löwen, Phys. Rev. Lett. **108**, 268307 (2012).
[25] H. H. Wensink and H. Löwen, J. Phys. Condens. Matter **24**, 464130 (2012).
[26] J. Elgeti and G. Gompper, Europhys. Lett. **85**, 38002 (2009).
[27] See Supplemental Material at http://link.aps.org/supplemental/10.1103/PhysRevLett.120.188002 for details on the rods and their properties, details of the numerical simulations, description of the theory and additional data about collisions between rods and with walls, the structure of the polar clusters, as well as details of the PDFs of clustering. It includes Refs. [28,29].
[28] F. Peruani and M. Bar, New J. Phys. **15**, 065009 (2013).
[29] S. Plimpton, J. Comput. Phys. **117**, 1 (1995).
[30] H.-P. Zhang, A. Be'er, E.-L. Florin, and H. L. Swinney, Proc. Natl. Acad. Sci. U.S.A. **107**, 13626 (2010).
[31] Y. Yang, V. Marceau, and G. Gompper, Phys. Rev. E **82**, 031904 (2010).
[32] S. Weitz, A. Deutsch, and F. Peruani, Phys. Rev. E **92**, 012322 (2015).
[33] A. Stukowski, Model. Simul. Mater. Sci. Eng. **18**, 015012 (2010).
[34] S. Redner, *A Guide To First- Passage Processes* (Cambridge University Press, Cambridge, England, 2001).
[35] A. M. Berezhkovskii and A. V. Barzykin, J. Chem. Phys. **136**, 054115 (2012).
[36] T. Calandre, O. Bénichou, and R. Voituriez, Phys. Rev. Lett. **112**, 230601 (2014).
[37] O. Bénichou, D. Grebenkov, P. Levitz, C. Loverdo, and R. Voituriez, Phys. Rev. Lett. **105**, 150606 (2010).
[38] A. G. Thompson, J. Tailleur, M. E. Cates, and R. A. Blythe, J. Stat. Mech. (2011) P02029.
[39] R. Soto and R. Golestanian, Phys. Rev. E **89**, 012706 (2014).
[40] A. B. Slowman, M. R. Evans, and R. A. Blythe, Phys. Rev. Lett. **116**, 218101 (2016).
[41] C. Scholz and T. Pöschel, Phys. Rev. Lett. **118**, 198003 (2017).
[42] E. Altshuler, J. M. Pastor, A. Garcimartín, I. Zuriguel, and D. Maza, PLoS One **8**, e67838 (2013).
[43] G. Junot, G. Briand, R. Ledesma-Alonso, and O. Dauchot, Phys. Rev. Lett. **119**, 028002 (2017).
[44] N. Nikola, A. P. Solon, Y. Kafri, M. Kardar, J. Tailleur, and R. Voituriez, Phys. Rev. Lett. **117**, 098001 (2016).
[45] Y. Fily, A. Baskaran, and M. F. Hagan, Soft Matter **10**, 5609 (2014).